Journal of the European Ceramic Society 16 (1996) 873–883

0955-2219(95)00213-8
0955-2219/96/$15.00 +.00

Reactions Occurring in Post Heat-Treated α/β Sialons: On the Thermal Stability of α-Sialon

Zhijian Shen,[a] Thommy Ekström[b] & Mats Nygren[b]

[a]Department of Materials Science and Engineering, Zhejiang University, Hangzhou 310027, People's Republic of China
[b]Department of Inorganic Chemistry, Arrhenius Laboratory, University of Stockholm, S-106 92 Stockholm, Sweden

(Received 29 September 1995; revised version received 23 November 1995; accepted 29 November 1995)

Abstract

To a powder mixture of an overall α-sialon composition $R_{0.4}Si_{10.2}Al_{1.8}O_{0.6}N_{15.4}$, *with* R= *Nd, Sm, Dy and Yb, were added extra amounts of powder mixtures, (20%), having Si:Al:*R *and O:N atomic ratios of 2:1:1 and 3:1, respectively. Series of α-rich mixed α/β-sialon ceramics containing about 20–30 vol% glassy phase were prepared from these powders by pressureless sintering at 1750°C. The as-prepared samples were subsequently heated at 1750°C and then quenched to room temperature or to 1150, 1300 and 1450°C (with a cooling rate exceeding 400°/min), and were annealed at these temperatures for various times. The samples quenched to room temperature revealed that α-sialon coexists with β-sialon and a liquid phase at 1750°C. The post heat-treatment at the lowest temperature involved a devitrification of the glassy phase and resulted in mixtures of mainly rare earth oxynitrides like the U-phase* $R_3Si_3Al_3O_{12}N_2$, *wollastonite* $RSiO_2N$ *or the B-phase* Dy_2SiAlO_5N. *Post heat-treatment at 1450°C induced a reaction between residual liquid and α-phase in the Nd- and Sm-systems and yielded a mixture of an oxygen- and a nitrogen-rich phase in all systems. Thus the melilite phase,* $R_2Si_{3-x}Al_xO_{3+x}N_{4-x}$, *is formed with all rare earth elements except Yb, which yields* $Yb_4Si_2O_7N_2$. *The oxygen-rich phase in the Nd- and Sm-systems was the aluminate* $RAlO_3$, *while in the Dy- and Yb-systems the garnet phase,* $R_3Al_5O_{12}$, *was formed. Similar results were obtained with samples quenched to 1300°C. These findings suggest that the stability of α-sialon is related to the type of sintering aid used. The phase assemblage found in the as-prepared samples is discussed in view of the findings obtained in the annealing experiments.*

1 Introduction

Sialon ceramics containing α- and/or β-sialon as the main constituents can be prepared by pressureless sintering when an excess of sintering aid(s) is used.[1–4] The observed high toughness of β-sialon is due to the presence of elongated β-crystals and an intergranular glassy phase: in tensile stresses, the cracks will follow tortuous pathways through the microstructure mainly within the latter phase.[5,6] However, the hardness of β-sialon ceramics, as well as the use of these materials at very high temperatures is restricted because of the presence of substantial amounts of residual glassy phase(s) in their microstructures.[4,7] Therefore, the α-sialon ceramics have attracted more attention recently, since they show excellent hardness and offer possibilities of reducing the amount of glassy phase by incorporating the constituents of sintering aids into the crystal lattice.[7,8] Post-sintering heat-treatment has become a frequently used technique for improving the high-temperature properties of sialon ceramics, as this procedure introduces a devitrification of the residual grain-boundary glassy phase.[9–11]

α-Sialon, isostructural with α-Si_3N_4, has an overall composition given by the formula $R_xSi_{12-(m+n)}Al_{m+n}O_nN_{16-n}$, where m(Si–N) are replaced by m(Al–N) and n(Si–N) by n(Al–O). The valence discrepancy introduced by the former substitution mechanism is compensated by the metal ion R^{p+}, where $m=px$.[12–15] The elements R of special interest for engineering α-sialon ceramics intended for use at high temperatures, are Y and the rare-earth elements Nd–Yb.[16] It has been shown that monophasic α-sialons samples are formed in a quite restricted compositional area, which does not vary extensively with the used R-element but does increase somewhat with decreasing size of the rare-earth cations.[14,17] Between the α-sialon plane and the β-sialon phase, $Si_{6-z}Al_zO_zN_{8-z}$, there is an area where α-and β-sialon phases coexist. These composition areas are quite similar in different R–Si–Al–O–N systems and are of special interest because, by carefully adjusting overall compositions

and using a transient liquid phase sintering route, a new kind of '*In situ* reinforced' or 'Self-reinforced' α–β sialon composite can be prepared, with only a minimum amount of residual glassy grain boundary phase.[18]

Recent results reported by different research groups have shown, however, that the α-sialon phase is thermodynamically unstable at lower temperatures in some *R*-sialon systems; i.e. in the presence of an intergranular liquid/glassy phase it tends to transform to β-sialon and other rare-earth-rich grain boundary phase(s).[10,19–21] The instability of the α-sialon at lower temperatures has been attributed to the smaller rare-earth cations being able to occupy the large voids present in the α-sialon structure at the sintering temperature, but not at lower temperatures.[10]

Our recent studies concerning the instability of the α-sialon phase in pure α- and duplex α–β-sialon systems have confirmed that $\alpha \rightarrow \beta$ transformations exist in different rare-earth doped sialon systems.[22–25] However, the decomposition pathway of α-sialon seems to be different in different systems, and it can be related to the preparation conditions used. These studies seem to indicate that the decomposition pathway depends on: (i) the size of the *R* ion; (ii) the composition of the α-sialon itself; (iii) the amount/ composition of the liquid present at the sintering temperature; (iv) the type/ amount of grain-boundary phase(s) formed during the cooling part of the sintering cycle, which in turn seems to depend on the cooling rate applied. Thus, in order to obtain an optimised microstructure all these factors need to be considered.

In this article we will describe the effect of the crystallization/devitrification of residual liquid/ glassy phase on the thermal stability of the α-sialon phase in different rare-earth doped sialon ceramics containing an excess amount of intergranular phase(s). For this purpose a series of α-rich α/β-sialons were prepared, containing an excess of added sintering aids. These materials were post heat-treated in different ways. In order be able to reveal the true phase composition at elevated temperatures and the thermal stability of the α-sialon phase at these temperatures, a furnace set-up was used which allowed very rapid cooling rates. Special attention will be paid to studies of the decomposition pathway of the α-sialon phase.

2 Experimental

α/β-Sialon compacts samples designed to have an excess of a glassy-phase (≥20 vol%) were prepared in the present work. To a powder mixture of the overall α-sialon composition $R_{0.4}Si_{10.2}Al_{1.8}O_{0.06}N_{15.4}$, with *R*= Nd, Sm, Dy and Yb, were added extra amounts of powder mixtures (20%) having Si:Al:*R* and O:N atomic ratios of 2:1:1 and 3:1, respectively. The designed overall compositions of the prepared samples (labelled GAR04 below) are summarised in Table 1.

Specimens were prepared from commercial Si_3N_4(UBE, SN-E10), AlN (H.C. Starck-Berlin, grade A), Al_2O_3 (Alcoa, A16SG), SiO_2 (99·9%, 325 mesh, Johnson Matthey Chemicals Ltd) and R_2O_3 (99·9%, Johnson Matthey Chemicals Ltd). The rare-earth oxide powders were calcined at 1000°C for 2 h before use. In the preparation of the samples, corrections were made for the small amounts of oxygen present in the Si_3N_4 and AlN raw materials. The starting material mixes were milled in water-free propanol for 24 h in a plastic jar, using sialon milling media, and the batch size used was 50 g. Pellets of dried powders (about 5 g) were first compacted in a steel die and then packed with a powder mixture of Si_3N_4, AlN and BN and pressureless sintered at 1750°C for 2 h in a graphite furnace in nitrogen atmosphere. The obtained samples were cooled to room temperature inside the furnace and are called as-prepared samples below.

Selected specimens were subsequently heat-treated in different ways. Some samples were placed in a carbon crucible embedded in the same powder bed as the one used above, and were re-heated up to 1750°C in a graphite furnace in nitrogen atmosphere. After 30 min holding time, the samples were either quenched to room temperature (at a rate of approximately 400°C/min. in the critical temperature range 1650–1000°C) by quickly moving them to a cooling chamber attached to the graphite furnace, or quenched to 1450, 1300, and 1150C, respectively. At these lower temperatures the samples were held for

Table 1. Overall compositions of the starting materials (in wt%)

Sample no.	Nd_2O_3	Sm_2O_3	Dy_2O_3	Yb_2O_3	Si_3N_4	*AlN*	Al_2O_3	SiO_2
GANd04	20·64	—	—	—	62·52	9·22	3·84	3·79
GASm04	—	21·14	—	—	62·21	9·14	3·79	3·72
GADy04	—	—	22·08	—	61·56	9·15	3·64	3·57
GAYb04	—	—	—	22·88	61·04	9·07	3·54	3·47

another 24 h (some samples were post heat-treated at 1450°C for extended times (up to 10 days)) and then quenched. The densities of the sintered specimens were measured according to Archimedes' principle.

The analyses of the crystalline phases present in the prepared samples were based on their X-ray powder diffraction records obtained in a Guinier-Hägg focusing camera with CuKα_1 radiation and Si as internal standard. The obtained photographs were evaluated with a computer-linked SCANPI system,[26] and the cell parameters were determined with the program PIRUM.[27] The z-value of the β-sialon phase, $Si_{6-z}Al_zO_zN_{8-z}$, was obtained from the unit cell dimensions of the samples, using the equations given in Ref. 28.

The phase transformations occurring in a given composition have been semi-quantitatively evaluated as a function of temperature and time have been applied. Thus, the $\alpha/(\alpha+\beta)$ ratio has been used to monitor the decomposition and formation of the α- and β-sialon phases, respectively; the M′/(M′ + A) ratio (M′ = the melilite solid solution $R_2Si_{3-x}Al_xO_{3+x}N_{4-x}$ and A-$RAlO_3$ with R=Nd, Sm and Dy) to monitor the formation of the M′ and A-phases; the M′/(M′ + G) ratio (G= samples of the garnet composition $R_3Al_5O_{12}$ with R=Dy, and Yb) to monitor the formation of the M′- and G-phases in the Dy-system and the G/(G+J) ratio (J=$Yb_4Si_2O_7N_2$) to monitor the formation of the G- and J-phases in the Yb-system. These ratios were obtained from the following relations:

$$\alpha/(\alpha+\beta) = I_{(\alpha)} / (I_{(\alpha)} + I_{(\beta)}) \quad (1(a))$$

$$M'/(M' + A) = I_{(M')} / (I_{(M')} + I_{(A)}) \quad (1(b))$$

$$M'/(M' + G) = I_{(M')} / (I_{(M')} + I_{(G)}) \quad (1(c))$$

$$G/(G+J) = I_{(G)} / (I_{(G)} + I_{(J)}) \quad (1(d))$$

where the integrated intensities $I_{(i)}$ of the following reflections were used: (i) (210) of the α-sialon; (ii) (210) of the β-sialon; (iii) (211) of the melilite solid solution (M′); (iv) (110) of the Nd aluminate, $NdAlO_3$, (200) of the Sm aluminate, $SmAlO_3$; (v) (420) of the garnet; $R_3Al_5O_{12}$ with R= Dy, and Yb; (vi) the peaks with d-values of 3·04 and 2·82 Å for the Yb J-phase, $Yb_4Si_2O_7N_2$.

After application of a carbon coating to the polished surfaces of the produced samples, these surfaces were examined in a scanning electron microscope (JEOL JSM 820, equipped with a Link AN 10000 EDS analyser). For some of the samples the Si, Al and R contents of the α-sialon grains and residual grain boundary glassy phase were determined by EDS analysis, using calibration curves. The final results reported below are averages of at least five experimental determinations.

3 Results and Discussion

3.1 Phase analysis of samples quenched from 1750°C to 1150, 1300 and 1450°C, respectively, and post heat-treated for various times

Crystallization/devitrification of the residual grain-boundary liquid/glassy phase may be achieved via two different post heat-treatment processes, namely, by heat-treatment above the glass transition temperature (T_g) but below the eutectic/liquid forming temperature of the glass, T_e, or by heat-treatment above T_e. The former process is in fact applied in conventional glass-ceramic industrial processes where the glass is devitrified at temperatures above its T_g point but below its softening temperature T_d. In this case the devitrification of the grain-boundary glass phase proceeds mainly within this phase, i.e. the main crystalline phases do not take part in the reactions. However, at temperatures exceeding T_e, a liquid is present in the material, and the crystallization of this liquid phase by heat-treatment in turn promotes reactions between this phase and the main crystalline phase(s), and in addition the liquid provides an effective diffusion pathway for the ions involved.

The liquid forming temperature (T_{lf}) in the R–Al–Si–O–N system is estimated to be around 1350°C,[10, 20, 21] and T_g and T_d of the glasses with the highest nitrogen content in these systems have been reported to be in the ranges 915–950°C and 960–1020°C, respectively.[30–32] Thus, based on these considerations, three post heat-treatment temperatures have been chosen, namely one above T_d but well below T_{lf} (1150°C), one just below T_{lf} (1300°C) and one well above T_{lf} (1450°C).

The XRD indications of phases present in samples quenched from 1750 to 1450°C (with holding times ranging from 4 to 240 h), 1300 (24 h), 1150°C (24 h) and to room temperature are given in Table 2. The table also contains observed unit cell parameters of the hexagonal α-sialon phase. The observed composition from EDS measurements of the α-sialon phase (the m, n and x-values in the formula $R_xSi_{12-(m+n)}Al_{m+n}O_nN_{16-n}$) and the Si, Al and R content in the glassy phase in samples quenched from 1750°C to room temperature are given in Table 3. The aimed-at and observed compositions of the α- and β-sialon are mapped out in Fig. 1. As α-sialon and β-sialon are in equilibrium with each other, the compositions of the obtained α-sialon are close to phase boundary, i.e. more oxygen-rich than the aimed-at composition.

Figures 2 and 3 show the SEM micrographs, obtained in back-scattered electron mode, of the samples quenched to room temperature from 1750°C and from 1450°C after annealing for 24 h.

Table 2. $\alpha/(\alpha+\beta)$ ratios and the crystalline grain boundary phases in samples post heat-treated under different conditions

Sample identification	$\alpha/(\alpha+\beta)$	*GB phase assemblage**								*α-sialon unit cell*	
		M′	*U*	*B*	*J*	*W*	*A*	*G*	*21R*	a(Å)	c(Å)
GANd04											
1750°C quenched	16·3	—	—	—	—	—	—	—	vw	7·814	5·694
1150°C/24 h	14·1	—	mw	—	—	s	—	—	vw	7·814	5·691
1300°C/24 h	0	m	—	—	—	—	s	—	vw	—	—
1450°C/4 h	0	s	w	—	—	—	m	—	vw	—	—
1450°C/24 h	0	s	—	—	—	—	ms	—	vw	—	—
1450°C/120 h	0	m	—	—	—	—	s	—	vw	—	—
1450°C/240 h	0	mw	—	—	—	—	s	—	vw	—	—
GASm04											
1750°C quenched	52·7	—	—	—	—	—	—	—	—	7·811	5·690
1150°C/24 h	34·8	—	w	—	—	mw	ms	—	—	7·810	5·690
1300°C/24 h	27·9	m	—	—	—	—	s	—	—	7·809	5·690
1450°C/4 h	28·8	s	vw	—	—	—	—	—	—	7·811	5·689
1450°C/24 h	3·6	s	—	—	—	—	—	—	—	—	—
1450°C/120 h	0	m					ms	—		—	—
1450°C/240 h	0	m	—	—	—	—	ms	—	—	—	—
GADy04											
1750°C quenched	79·5	ms	—	—	—	—	—	—	—	7·807	5·688
1150°C/24 h	70·1	m	—	w	—	—	m	—	—	7·807	5·687
1300°C/24 h	72·2	m	—	—	—	—	—	s	—	7·805	5·687
1450°C/4 h	57·5	ms	—	—	—	—	—	w	—	7·805	5·684
1450°C/24 h	47·0	s	—	—	—	—	—	mw	—	7·805	5·689
1450°C/120 h	45·0	m	—	—	—	—	—	ms	—	7·805	5·690
1450°C/240 h	36·2	m	—	—	—	—	—	ms	—	7·807	5·688
GAYb04											
1750°C quenched	78·1	—	—	—	—	—	—	—	—	7·804	5·682
1150°C/24 h	61·2	—	—	—	w	—	ms	—	—	7·804	5·683
1300°C/24 h	59·8	—	—	—	w	—	—	s	—	7·800	5·682
1450°C/4 h	64·3	—	—	—	w	—	—	s	—	7·802	5·681
1450°C/24 h	55·7	—	—	—	w	—	—	vs	—	7·800	5·682
1450°C/120 h	55·1	—	—	—	w	—	—	vs	—	7·801	5·683
1450°C/240 h	57·3	—	—	—	w	—	—	vs	—	7·801	5·682

*M′ = the melilite solid solution $R_2Si_{3-x}Al_xO_{3+x}N_{4-x}$ with R=Nd, Sm and Dy; U = the U-phase $R_3Si_3Al_3O_{12}N_2$ with R=Nd, and Sm; B = the B-phase Dy_2SiAlO_5N; J = the J-phase $Yb_4Si_2O_7N_2$; W = the wollastonite phase $RSiO_2N$ with R=Nd, and Sm; A = the aluminate phase $RAlO_3$, with R=Nd, Sm, Dy, Yb; G, the garnet phase $R_3Al_5O_{12}$ with R= Dy, and Yb; 21R = the 21R polytype $Si_xAl_{7-x}O_{3-x}N_{6+x}$.
X-ray intensities: s = strong; m = medium; w = weak; vw = very weak.

Table 3. Composition of the α- and grain-boundary glassy phases, as determined by EDS. The compositions of the precursor powders are also given

Sample	*α-sialon*			*Glassy phase*		
	m	n	x	*Si*	*Al*	R(at %)
Precursor composition	1·2	0·6	0·4	50	25	25
GANd04	1·38	0·39	0·46	45	20	35
GASm04	1·14	0·82	0·38	41	27	32
GADy04	1·11	0·80	0·37	52	20	28
GAYb04	1·11	1·19	0·37	24	52	24

The black areas are β-sialon or 21R polytype grains, the medium grey areas represent α-sialon, and the bright ones a glass phase and/or crystallized rare-earth-rich intergranular phases. It is obvious that the samples quenched from 1750°C predominantly contain elongated β-sialon grains and equiaxied α-sialon grains surrounded by a residual glassy phase. An increase of the amount of the α-sialon and a decrease of the amount of grain-boundary glassy phase with decreasing ion radius of the cation size can also be discerned. Rare-earth-rich crystalline phases, which tend to

segregate into certain areas (see Fig. 3(e)), are formed after annealing at 1450°C for 24 h.

Before discussing the crystallization/devitrification process of the intergranular liquid/glassy phase, the following general observations concerning the thermal stability of the α-sialon phase can be made:

(i) All samples quenched from 1750°C to room temperature contained α- and β-sialon grains and a glassy phase. Additional crystalline grain-boundary phases were only found in the Nd- and Dy-systems, namely 21*R* (in minor amounts) and melilite, respectively.

(ii) The $\alpha/(\alpha+\beta)$ ratio increases with decreasing radius of the R ion in samples quenched from 1750°C to room temperature, e.g. in the order Nd, Sm, Dy and Yb.

(iii) The thermal stability of the α-phase at 1450°C decreases drastically with increasing radius of the *R* ion. In fact, after 240 h post heat-treatment, no α phase is left in the Nd- and Sm-systems, and a decrease of the $\alpha/(\alpha+\beta)$ ratio with the number of hours of heat-treatment is seen in the Dy- and Yb-systems. The main part of the latter decrease is, however, probably due to the β-phase being formed during the devitrification process (see below and Figs. 3(a–d)).

(iv) The lattice parameters of the α-sialon phase vary with the *R* ion used in an expected manner, but they do not seem to vary with temperature or duration of the post heat-treatment within each system, i.e. the composition of the α-phase does not vary with time and temperature of the post heat-treatment. Such a compositional variation has previously been reported to occur in the Nd- and Sm-systems implying that the α-phases

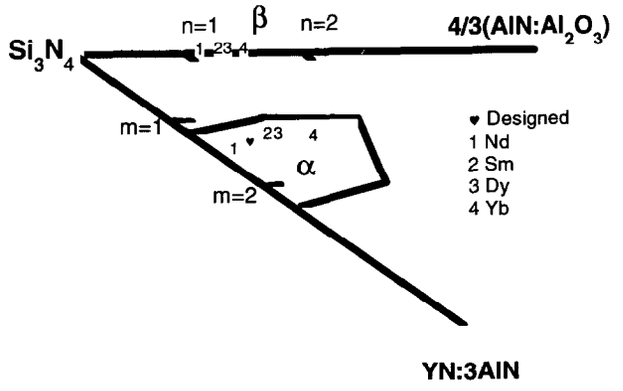

Fig. 1. A schematic illustration of the α-sialon plane in a Jänecke prism of *R*–Si–Al–O–N systems. The location of the designed α-sialon overall composition and the measured compositions of formed α- and β-sialon phases are marked.

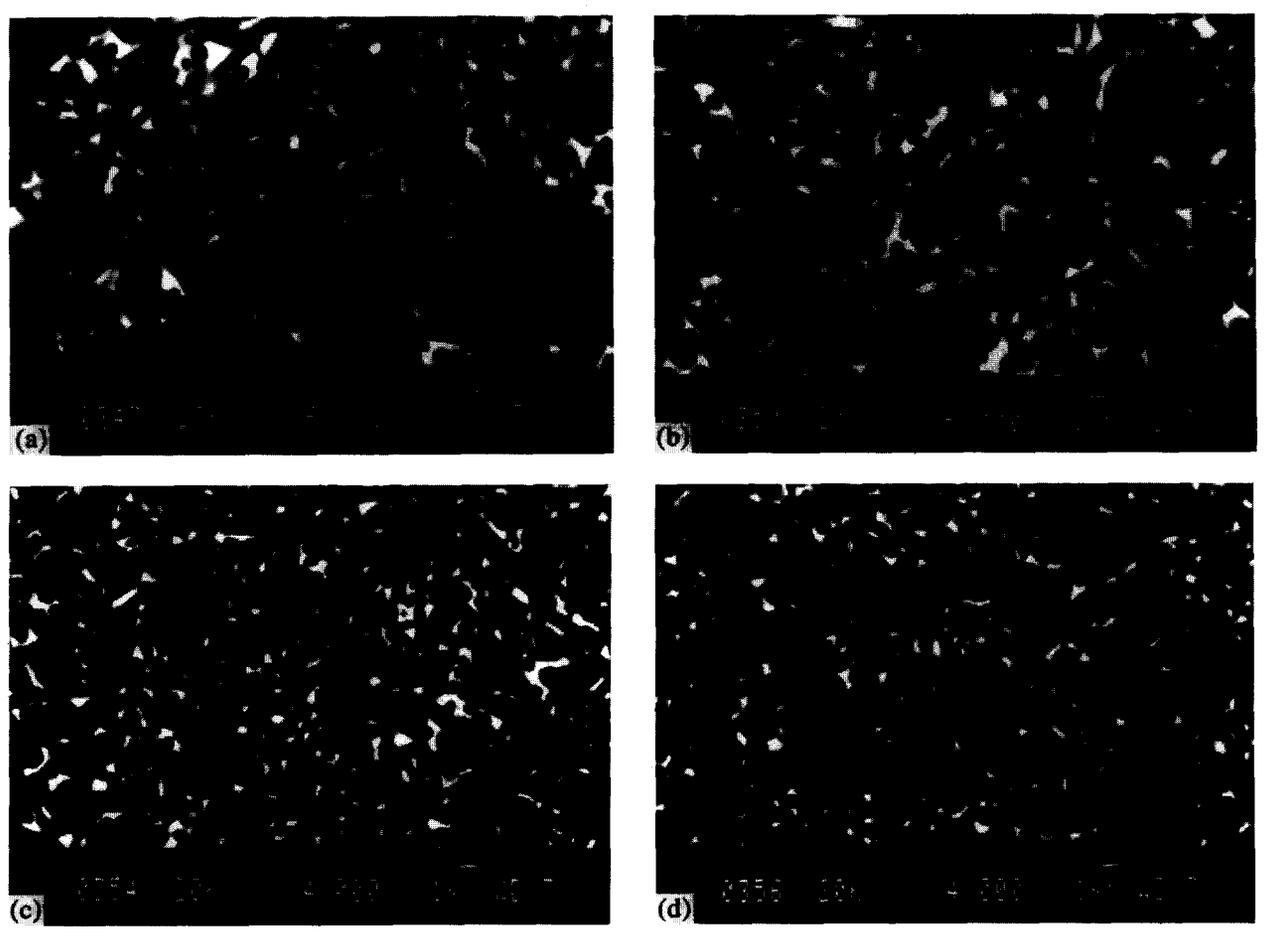

Fig. 2. SEM micrographs obtained in back scattered electron mode, illustrating the microstructure of samples quenched from 1750°C: (a) *GA*Nd04; (b) *GA*Sm04, (c) *GA*d04, and (d) *GA*Yb04.

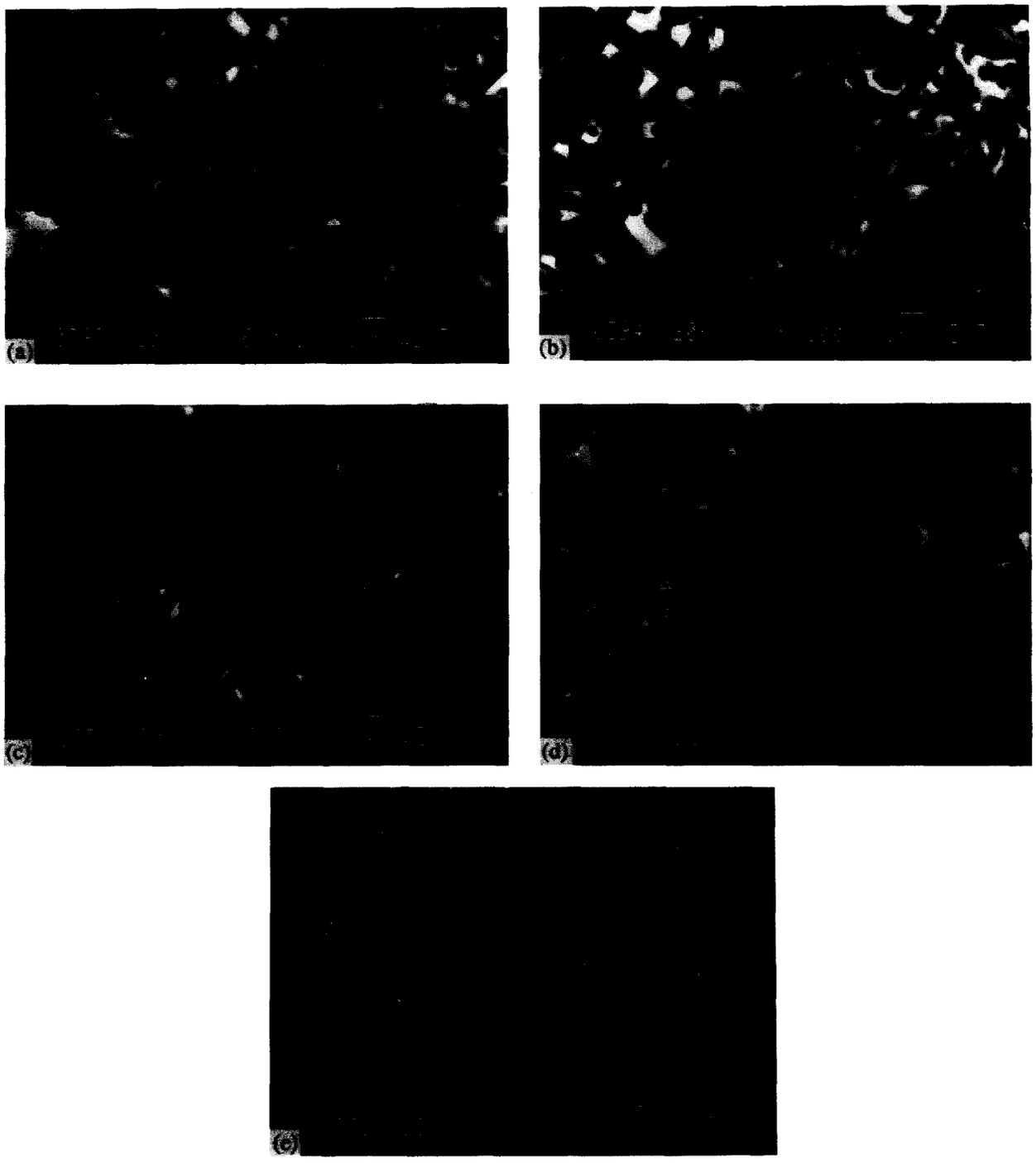

Fig. 3. SEM micrographs of samples heat-treated at 1450°C for 24 h: (a) *GA*Nd04, (b) *GA*Sm04; (c) *GA*Dy04 and (d) *GA*Yb04. The low-magnification micrograph of *GA*Dy04 shows agglomerates of the formed crystalline grain-boundary phases in (e).

lost *R*-elements upon prolonged annealing before they decomposed.[22,23] The compositions of the present α-sialon phases are, however, very close to the borderline of the α-phase area, as seen in Table 3 and Fig. 1, which in turn implies that we cannot expect any compositional variation in the present systems.

3.1.1 Heat-treatment of Nd-sialons

As mentioned above, the samples in the Nd-system, which were quenched from 1700°C to room temperature, contained minor amounts of the 21R phase, and so did all post heat-treated samples. The α-phase in this system decomposes very rapidly at 1450°C. Thus there is no α-phase left after 4 h post heat-treatment, but melilite (M′), $NdAlO_3$ (A) and minor amounts of the U-phase, $R_3Si_3Al_3O_{12}N_2$ are. Prolonged heat-treatment decomposes the U-phase, and more and more A-phase is formed; but if the amount of M′-phase decreases, it decreases at a lower rate than the A-phase is formed. The decrease in the M′(M′+A) ratio with increasing holding times, illustrated in Fig. 4(a), is thus mainly due to progressing A-phase formation. For stoichiometric

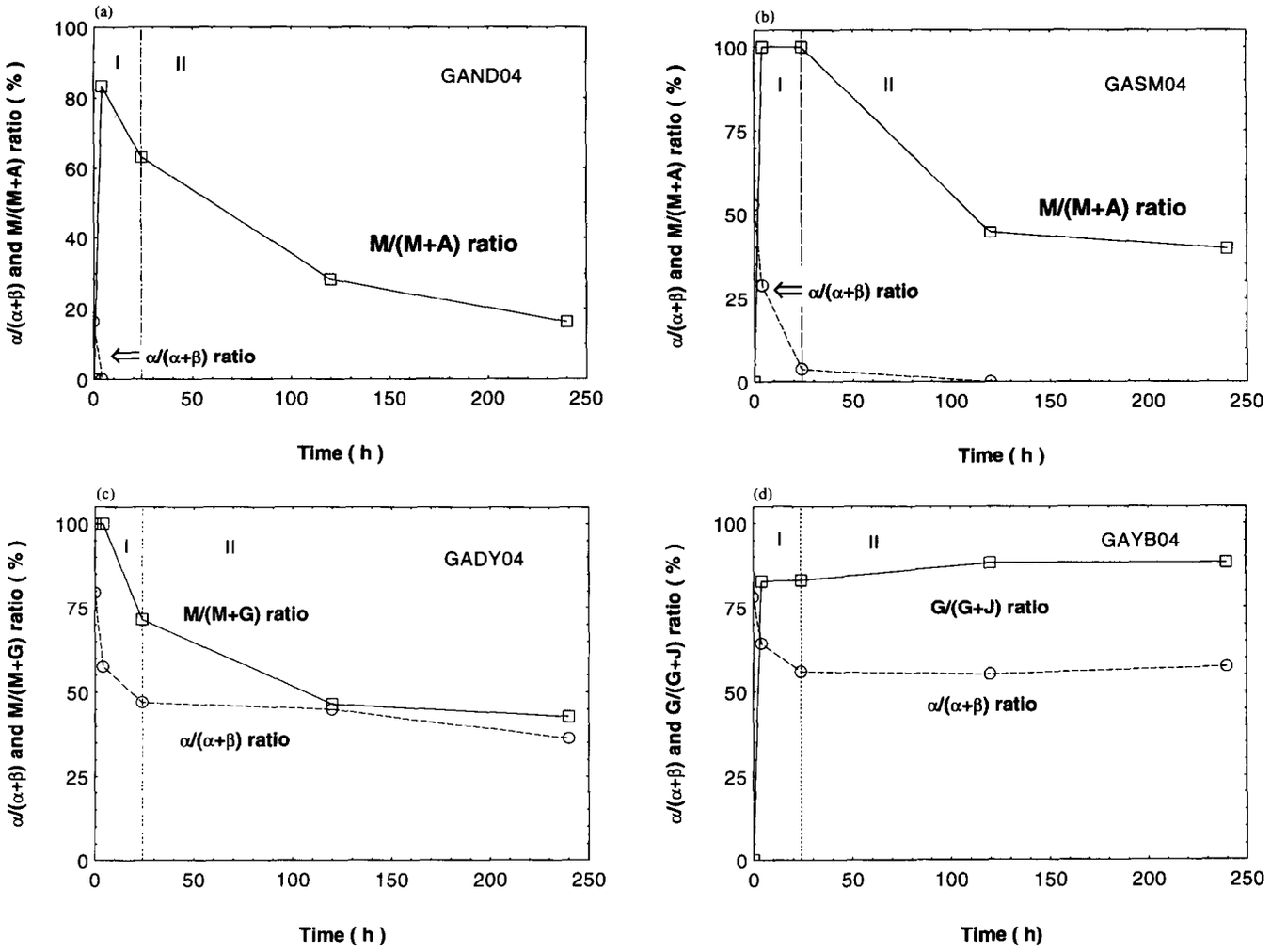

Fig. 4. $\alpha/(\alpha+\beta)$ ratio and grain-boundary phase formation plotted as funtion of the annealing time at 1450°C: (a) *GA*Nd04; (b) *GA*Sm04; (c) *GA*Dy04, and (d) *GA*Yb04.

reasons, β-sialon must also be formed in connection with these reactions. At 1450°C, the crystallization process in the Nd-system thus seems to proceed according to the following pathway:

$$L_1 + \alpha \rightarrow L_2 + M' + A + U + \beta \rightarrow A + M' + \beta \quad (2)$$

where L_1 and L_2 are liquids of different compositions and volume. The final crystallization products besides β-sialon are one pure oxide (A) and one N-rich phase (M′)

At 1300°C, and after 24 h annealing, there is no α-sialon phase left, but some M′-phase and more A-phase has formed. Simultaneously β-sialon is formed for the same reasons as above, yielding an overall devitrification pathway of:

$$\text{Glass} + \alpha \rightarrow A + M' + \beta \quad (3)$$

A quite different phase assembly was observed in the samples post heat-treated at 1150°C for 24 h. The devitrification process at this temperature forms wollastonite, $R\text{SiO}_2\text{N}$, (abbreviated as W below) and the U-phase, $R_3\text{Si}_3\text{Al}_3\text{O}_{12}\text{N}_2$, and because approximately the same $\alpha/(\alpha+\beta)$ ratio is found in this sample as in samples quenched from 1750°C to room temperature (see Fig. 5), this devitrification process does not seem to involve the α-phase, but follows the pathway:

$$\text{Glass} \rightarrow W + U \quad (4)$$

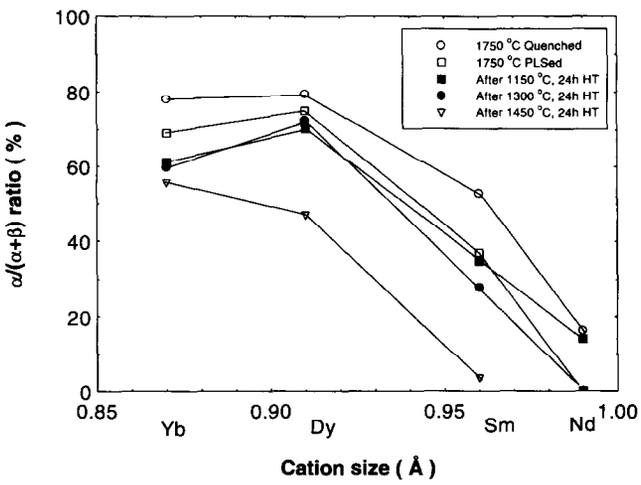

Fig. 5. The $\alpha/(\alpha+\beta)$ ratio in samples exposed to different heat-treatments plotted versus the ion radius of the *R*-ion.

3.1.2 Heat-treatment of Sm-sialons

In the Sm-system, samples quenched from 1750 to 1450°C and annealed at the latter temperature for 4 h did contain α-phase, but the $\alpha/(\alpha+\beta)$ ratio decreased from 52·7 to 28.8% while the M′-phase and minor amounts of the U-phase were simultaneously formed. Upon further heat-treatment, the α-phase and the U-phase were decomposed, and initially more M′ was formed, but later in the crystallization process the A-phase formed and the M′/(M′ + A) ratio remained almost constant from 120 h heat-treatment and further on as seen in Fig. 4(b). As above, β-sialon formed simultaneously. The suggested crystallization pathway at this temperature is thus:

$$L_1 + \alpha \rightarrow L_2 + \mathrm{M}' + \mathrm{U} + \beta \rightarrow \mathrm{M}' + \mathrm{A} + \beta \quad (5)$$

The liquid L_2 has a different composition and volume than L_1. The final crystallization products are the same as above for R=Nd, i.e. one oxygen- and one nitrogen-rich phase.

At 1300°C, and after 24 h post heat-treatment, the A- and β-phases were formed, but $\alpha/(\alpha+\beta)$ ratio was almost the same as after 4 h annealing at 1450°C. Thus, if the α-phase does decompose, its decomposition is substantially lower at this temperature, suggesting the following devitrification pathway:

$$\mathrm{Glass} + (\alpha) \rightarrow \mathrm{M}' + \mathrm{A} + \beta \quad (6)$$

Again, as above, a quite different phase assembly was observed in the samples post heat-treated at 1150°C for 24 h The devitrification process at this temperature thus produces the A-, W- and U-phases. The formation of these phases implies that the β-sialon phase must also be formed. Thus, the decrease in the $\alpha(\alpha+\beta)$ ratio of this sample, compared with that of samples quenched to room temperature from 1750°C (see Fig. 5), might be due to an increasing content of the β-phase. If this assumption is true, our observations suggest the following devitrification pathway at 1150°C in this system:

$$\mathrm{Glass} \rightarrow \mathrm{A} + \mathrm{W} + \mathrm{U} + \beta \quad (7)$$

Post heat-treatment of Sm-sialon compounds has to some extent been studied previously, and it can be concluded that our findings are in agreement with previous results.[9,10]

3.1.3 Heat-treatment of Dy-sialons

It is surprising that the M′-phase is observed in samples in the Dy-system quenched from 1750°C to room temperature. This suggests that the Dy-M′-phase would be thermally more stable than its Nd- and Sm-counterparts, contrary to the general opinion that the thermal stability of the M′-phase decreases with decreasing ionic radius of the R ion. Another possibility would be that the M′-phase present in the as-prepared sample (see below) for some reason did not dissolve during the subsequent heat-treatment at 1750°C. Additional studies to confirm this observation are needed. Anyhow, the α-phase is thermally more stable in this system than in the Nd and Sm ones, as a substantial amount of this phase remains in the sample after annealing at 1450°C for 240 h. A comparison of the $\alpha/(\alpha+\beta)$ ratio in the samples quenched to room temperature and annealed for 4 h at 1450°C suggests that the α-phase is initially involved in the crystallization process. The decrease of the $\alpha/(\alpha+\beta)$ ratio with increasing holding times can be explained by the observation that more β-sialon is formed in conjunction with a grain boundary phase of garnet composition $Dy_3Al_5O_{12}$(G), while the amount of the M′-phase is seemingly constant (see Fig. 4(c)). This suggests that the crystallization process in the Dy-system and in presence of a liquid initially follows the pathway:

$$L_1 + \alpha \rightarrow \mathrm{M}' + \mathrm{G} + \beta \quad (8)$$

while in the latter part of the crystallization process it seems that the dominating reaction is the formation of the G-phase and that this process occurs without the α-phase being involved. The pure oxide phase for Dy is a garnet instead of an aluminate structure, as observed above for Nd and Sm. This is in agreement with earlier findings.[9,10]

Samples annealed at 1300°C for 24 h exhibited almost the same $\alpha/(\alpha+\beta)$ ratio and M′ content as that found in samples quenched to room temperature, but they contained in addition a substantial amount of the G-phase. These observations suggest that the α-phase is not involved in the devitrification process in the glass at 1300°C in the Dy-system, which proceeds as:

$$\mathrm{Glass} \rightarrow \mathrm{G} + \beta \quad (9)$$

The phase assembly observed in the samples post heat-treated at 1150°C for 24 h is quite different from that observed at higher temperatures. The devitrification process at this temperature thus produces A-phase and minor amounts of a grain boundary phase of the composition Dy_2SiAlO_5N (B). The formation of these phases implies that the β-sialon phase must also form, and that the decrease in the $\alpha/(\alpha+\beta)$ ratio in this sample, compared with that of samples quenched to room temperature from 1750°C (see Fig. 5), is most probably due to an increasing content of the β-phase, suggesting the following devitrification pathway:

$$\mathrm{Glass} \rightarrow \mathrm{A} + \mathrm{B} + \beta \quad (10)$$

3.1.4 Heat-treatment of Yb-sialons

Yb does not form any M′-phase, and the most stable grain boundary phase in this system is the G-phase. It is formed in large amounts already after 4 h annealing at 1450°C, in conjunction with the β-phase and minor amounts of $Yb_4Si_2O_7N_2$ (J). The variation of the $\alpha/(\alpha+\beta)$ and G/(G +J) ratios (see Fig. 4(d)) with annealing time indicates that, if the α-phase is involved in the crystallization process, the amount which is decomposed is very small and that, if so, this decomposition occurs only in the very beginning of the process. Furthermore, the rate of crystallization seems to be faster in this system than in the others, as these ratios become almost constant after 24 h annealing. This suggests the following crystallization pathway:

$$L_1 + (\alpha) \rightarrow G + \beta + J \qquad (11)$$

The same pathway seems to be operative at 1300°C, while at 1150°C the devitrification product is A-phase instead of the G-phase.

3.1.5 Concluding remarks concerning the crystallization/devitrification pathway

From these observations it can be concluded:

(i) At least two grain boundary phases are formed in each system: one nitrogen-rich and one oxygen-rich. The N-rich melilite $R_2Si_{3-x}Al_xO_{3-x}N_{4-x}$ is formed for all rare earth elements, except Yb which forms J-phase ($Yb_4Si_2O_7N_2$). The observed oxide was an aluminate ($RAlO_3$) for Sm/Nd and a garnet ($R_3Al_5O_{12}$) for Dy/Yb.

(ii) The phase assembly formed by devitrification of the intergranular glass phase at temperatures slightly above the softening temperature (1150°C) is quite different from that appearing in samples annealed slightly below its liquid-forming temperature (1300°C), which in turn resembles that obtained at temperatures above T_{lf}(1450°C).

(iii) The α-phase is not involved in the devitrification taking place at 1150°C.

(iv) In the Nd- and Sm-systems, the M′- and A-phases are thermodynamically more stable than the α-phase, i.e. at elevated temperatures (T>1150°C) the α-phase decomposes.

(v) If the α-phase is take part in the reactions during the crystallization/devitrification processes in the Dy- and Yb-systems, it does so in the very beginning of the processes and in a limited amount, i.e. the α-phase seems to be thermodynamically stable in these systems.

3.2 Phase analysis of as-prepared samples

The overall composition of the designed sample corresponded to an 80 vol% α-sialon (of the composition GAR04) and a 20 vol% glass content (with a Si:Al:R ratio equal to 2:1:1 and O:N = 3:1). This sample after being pressureless-sintered at 1750°C and cooled to room temperature at a rather slow rate, yielded α/β-sialon ceramics containing about 20–30 vol% glassy phase and different kinds of crystalline grain boundary phases. The phases formed, the lattice parameters of the α- and β-phases and the $\alpha/(\alpha+\beta)$ ratio are shown in Fig. 5 and given in Table 4, respectively.

The phase analysis showed that the Nd sample did not contain any α-phase, but substantial amounts of the M′-phase and minor amounts of the U-phase. The α-phase is present in the Sm sample, but the $\alpha/(\alpha+\beta)$ ratio is lower than those found in the Dy- and Yb-samples. In the Sm sample the M′- and U-phases occur as grain boundary phases, while the M′- and B-phases are formed in the Dy sample. Finally, in the Yb sample the only intergranular phase is the J-phase.

The observation that extremely small amounts of α-phase are present in the Nd sample is in agreement with the annealing experiments, which showed that the α-phase is decomposed in this system. The U- and B-phases are only formed in the low-temperature region (1150°C) in the annealing experiments, while the J-phase is formed both at high and low temperatures. As mentioned above, we always observed one oxygen-rich and one nitrogen-rich phase at the end of our annealing experiments.

Table 4. $\alpha/(\alpha+\beta)$ ratio, grain-boundary phase assemblage and unit cell dimensions of α- and β-sialon in as-prepared samples

Samples	*Density* (g/cm^3)	α/(α+β) (%)	*GB* phase assemblage*					α			β		
			M	*J*	*B*	*U*	*21R***	a(Å)	c(Å)	x***	a(Å)	c(Å)	z***
GAND04	3·566	0	s	—	—	w	w	—	—	—	7·6198	2·9194	0·53
GASM04	3·588	37	ms	—	—	m	—	7·8102	5·6897	0·42	7·6246	2·9203	0·62
GADY04	3·675	75	m	—	m	—	—	7·8070	5·6873	0·39	7·6249	2·9217	0·65
GAYB04	3·681	69	—	mw	—	—	—	7·8032	5·6835	0·40	7·6302	2·9204	0·72

Remarks: *GB, grain boundary; ***M*, Melilite $R_2Si_{3-x}Al_xO_{3-x}N_{4-x}$ with R=Nd, Sm and Dy; *J*, *J*-phase $Yb_4Si_2O_7N_2$;*B*, *B*-phase Dy_2SiAlO_5N; *U*, *U*-phase $R_3Si_3Al_3O_{12}N_2$ with R=Nd, and Sm; ***α-sialon x-value and β-sialon z-value calculated according to the unit cell dimensions.

X-ray intensities: s, strong; m, medium; w, weak.

In this connection it is interesting to note that no oxygen-rich grain-boundary phase is formed in the as-prepared samples. This observation suggests that the oxygen-rich phases are not formed as long as the nitrogen content of the liquid/glass is high, i.e. nitrogen-rich phases are formed first in the crystallization/devitrification process, and when the oxygen content of the liquid/glass has become high enough, the crystallisation of oxygen-rich intergranular phases starts. The fact that we do not observe any oxygen-rich phases in our as-prepared samples can thus be understood to mean that the cooling rate was too high to allow a more oxygen-rich glassy phase to form.

Our observations thus suggest that the crystallization process in as-prepared samples in the Nd- and Sm-systems follows the pathway:

$$L_1 + \alpha \rightarrow L_2 + M' + U + \beta \quad (12)$$

in the Dy-system:

$$L_1 + M' \rightarrow M' + B + \beta \quad (13)$$

and in the Yb-system:

$$L_1 \rightarrow J + \beta \quad (14)$$

4 Concluding Remarks

As shown above, α-sialon coexists with β-sialon and a liquid phase at 1750°C in Nd-, Sm-, Dy and Yb doped systems, but in the cases of Nd and Sm the α-phase decomposes at lower temperatures. This behaviour has also been observed for Nd- and Sm-α-sialon ceramics containing substantially smaller amounts of intergranular liquid/glassy phases.[22,23] The crystallization/devitrification rate seems to be much faster, though, when the samples contain an excess of the liquid/glass phase, in accordance with earlier indications.[19] If the decomposition of the α-phase is only triggered by the formation of the M′-phase, it is difficult to understand why decomposition does occur in the Nd- and Sm-systems but not with Dy. The Dy-M′-phase can accommodate substantially less Al in its lattice than the Nd- and Sm-M′-phases,[33] and one may speculate that the decomposition rate of the α-phase in the Dy-system is retarded because the formed liquid would otherwise be too Al-rich (see also below). In this connection it should be noted that if one could prepare a Nd- or Sm-α-sialon ceramic without intergranular glass, the α-phase ought to be stable for stoichiometric reasons, because a very nitrogen-rich liquid/glass must be formed besides the M′-phase, and thus seems impossible. The highest observed N-content in a Sm-glass is slightly above 40 eq%.[34]

Our findings show that the phase assembly obtained in as-prepared samples is strongly dependent on: (i) the type of R_2O_3 used as sintering aid; (ii) the amount and composition of the liquid phase formed at the sintering temperature; and (iii) to a greater extent than has previously been realized, on the cooling rate applied.

If the liquid phase formed is nitrogen-rich, as it seems to be in our systems, a nitrogen-rich intergranular phase is formed before an oxygen-rich one, because otherwise the liquid would become too nitrogen-rich. Accordingly, the temperature dependence of the composition variability of the liquid/glass *vis à vis* nitrogen and Al (see above) must also be considered when preparing an α/β-sialon ceramic with designed grain boundary phase(s).

Acknowledgements

This study has been supported by the Swedish Research Council for Engineering Sciences. Zhijian Shen thanks the Swedish Institute for a scholarship during the period when the work was carried out.

References

1. Jack, K. H., Review: Sialons and Related Nitrogen Ceramics, *J. Mater. Sci.*, **11** (1976) 1135–58.
2. Lewis, M. H., Ward, G. & Jasper, C., Sintering Additive Chemistry in Controlling Microstructure and Properties of Nitrogen Ceramics. *Ceram. Powder Sci.*, **2** (1988) 1019–33.
3. Ekström, T., Effect of Composition, Phase Content and Microstructure on the Performance of Yttrium SiAlON Ceramics. *Mater. Sci. Eng.*, **A109** (1989) 341–9.
4. Ekström T. & Nygren, M., Sialon Ceramics. *J. Am. Ceram. Soc.*, **75** (1992) 259–76.
5. Becher, P. F., Microstructural Design of Toughened Ceramics. *J. Am. Ceram. Soc.*, **74** (1991) 255–69.
6. Ekström, T., SiAlON Composite Ceramics. In *Tailoring of Mechanical Properties of Si_3N_4 Ceramics*, ed. M. J. Hoffmann & G. Petzow. Kluwer Acad. Publ., Netherlands, 1994, pp. 149–61.
7. Ekström, T., Hardness of Dense Si_3N_4-Based Ceramics. *J. Hard Mater.*, **4** (1993) 77–95.
8. Cao, G. Z. & Metselaar, R., α-SiALON Ceramics: a review, *Chem. Mater.*, (1991) 242–52.
9. Mandal, H., Thompson, D. P. & Ekström, T., Heat treatment of sialon ceramics densified with higher atomic number rare earth and mixed yttrium/rare earth oxides. In *Proc. Special Ceramics 9*, The Institute of Ceramics, Stoke-on-Trent, UK, 1992, pp. 97–104.
10. Mandal, H., Thompson, D. P. & Ekström, T., Reversible α-β-Sialon Transformation in Heat-treated Sialon Ceramics. *J. Europ. Ceram. Soc.*, **12** (1993) 421–9.
11. Mandal, H., Cheng, Y. B. & Thompson, D. P., α-sialon Ceramics with a Crystalline Melilite Grain-Boundary Phase, Aluminium-Containing Nitrogen Melilite. In *5th International Symposium on Ceramic Materials and Components for Engines*, ed. D. S. Yan, X. R. Fu & S. X. Shi. World Scientific, Singapore, 1995, pp 202–5.

12. Hampshire, S., Park, H. K., Thompson, D. P. & Jack, K. H., α′-Sialon Ceramics, *Nature* (London), **274** (1978) 880–2.
13. Jack, K. H., Silicon Nitride, Sialons, and Related Ceramics. In *Ceramics and Civilization Vol. III, High-Technology Ceramics.* American Ceramic Society, Columbus, OH, 1986, pp. 259–88.
14. Sun, W. Y., Tien, T. Y. & Yen, T.-S., Solubility Limits of α′-Sialon Solid Solutions in the System Si, Al, Y / N, O. *J. Am. Ceram. Soc.*, **74** (1991) 2547–50.
15. Stutz, D., Greil, P. & Petzow, G., Two-Dimensional Solid-Solution Forming of Y-Containing α-Si_3N_4. *J. Mater. Sci. Letters,* **5** (1986) 335–6.
16. Ekström, T., Sialon Ceramics Sintered with Yttria and Rare Earth Oxides. *Mat. Res. Soc. Symp. Proc.,* **287** (1993) 121–32.
17. Huang, Z. K., Tien, T. Y. & Yen, T. S., Subsolidus Phase Relationships in Si_3N_4–AlN–Rare Earth Oxide Systems. *J. Am. Ceram. Soc.*, **69** (1986) C-241–42.
18. Ekström, T., Shen, Z.-J. & Falk L., Dysprosium and Samarium Doped α-β Sialon Ceramics with a Minimum of Residual Glass, submitted to *J. Am. Ceram. Soc.*
19. Ekström T. & Shen, Z.-J. Temperature Stability of Rare Earth Doped α-Sialon Ceramics. In *5th Intern. Symp. on Ceramic Materials and Components for Engine*, ed. D. S. Yan, X. R. Fu & S. X. Shi. World Sci. Publ. Co., 1995, pp. 206–10.
20. Cheng, Y. B. & Thompson, D. P., Preparation and Grain Boundary Devitrification of Samarium α-Sialon Ceramics. *J. Europ. Ceram. Soc.*, **14** (1994) 13–21.
21. Zhao, R. & Cheng, Y., Phase Transformations in Sm(α+β)-SiAlON Ceramics during Post-Sintering Heat Treatments, submitted to *J. Euro. Ceram. Soc.*
22. Shen, Z.-J., Ekström, T. & Nygren, M., Temperature Stability of Samarium Doped α-Sialon Ceramics. *J. Europ. Ceram. Soc.*, **16** (1996) 43.
23. Shen, Z.-J., Ekström, T. & Nygren, M., Homogeneity Region and Thermal Stability of Neodymium Doped α-Sialon Ceramics. *J. Am. Ceram. Soc.*, **79** (1996) 721.
24. Shen, Z.-J., Ekström T. & Nygren, M., Ytterbium Stabilised α-Sialon Ceramics. *J. Phys D: Appl. Phys*, **29** (1996) 893.
25. Shen, Z.-J., Ekström, T. & Nygren, M., Preparation and Properties of Stable Dysprosium Doped α-Sialon Ceramics. Submitted to *J. Mater. Sci.*
26. Anstis, G. R., Chantikul, P., Lawn, B. R. & Marshall, D. P., A Critical Evaluation of Indentation Techniques for Measuring Fracture Toughness: I, Direct Crack Measurements. *J. Am. Ceram. Soc.*, **64** (1981) 533.
27. Johansson, K.-E., Palm, T & Werner, P.-E., An Automatic Microdensitometer for X-ray Powder Diffraction Photographs. *J. Phys.*, **E13** (1980) 1289–91.
28. Werner, P.-E., A Fortran Program for Least-Squares Refinement of Crystal Structure Cell Dimension, *Arkiv för Kemi*, **31** (1969) 513.
29. Ekström, T., Käll, P.-O., Nygren, M. & Olsson, P.-O., Dense Single-Phase β-Sialon Ceramics by Glass-Encapsulated Hot Isostatic Pressing. *J. Mater. Sci.*, **24** (1989) 1853–61.
30. Hampshire, S., Drew, R. A. L. & Jack, K. H., Oxynitride glasses. *Phys. Chem. of Glasses*, **26** (1985) 182–6.
31. Murakami, Y. & Yamamoto, H., Properties of Oxynitride Glasses in the Ln–Si–Al–O–N Systems (Ln=Rare-Earth), *J. of the Ceram. Soc. of Japan, Int. Edition*, **102** (1995) 234–8.
32. Mandal, H., Thompson, D. P. & Ekström, T., Heat Treatment of Ln–Si–Al–O–N glasses. In *Proc. 7th Irish Mater. Forum Conf. IMF7*, ed. M. Buggy & S. Hampshire. Trans. Tech Publications, Switzerland, 1992, pp. 187–203.
33. Wang, P. L., Tu, H. Y., Sun, W. Y., Yan, D. S., Nygren, M. & Ekström, T., On the Solid Solubility of Al in the Melilite Systems $R_2Si_{3-x}Al_xO_{3+x}N_{4-x}$ with R=Nd, Sm, Gd, Dy, and Y. *J. Europ. Ceram. Soc.*, **15** (1995) 689.
34. Tu, H. U., Sun, W. Y., Wang, P. L. & Tan, D. S., Glass-forming region in the Sm–Si–Al–O–N system, *J. Mater. Sci. Letters,* **14** (1995) 1118–22.